Femoral neck cortical bone distribution in *Nacholapithecus* from the Middle Miocene of Kenya

Yuma Tomizawa[a,*], Marta Pina[b, c], Yasuhiro Kikuchi[d], Naoki Morimoto[a], Masato Nakatsukasa[a]

[a] *Laboratory of Physical Anthropology, Graduate School of Science, Kyoto University, Kyoto, 606-8502, Japan*

[b] *South Bank Applied BioEngineering Research (SABER), School of Engineering, London South Bank University, SE1 OAA, UK*

[c] *Institut Català de Paleontologia Miquel Crusafont, Universitat Autònoma de Barcelona, C/ Columnes S/n, Campus de La UAB, 08193, Cerdanyola Del Vallès, Spain*

[d] *Division of Human Anatomy and Biological Anthropology, Department of Anatomy and Physiology, Faculty of Medicine, Saga University, Saga, 849-8501, Japan*

[*] **Corresponding author.**

E-mail addresses: tomizawa@anthro.zool.kyoto-u.ac.jp (Y. Tomizawa).

Acknowledgments

We thank the National Museums of Kenya (Earth Sciences Department) for permission to study specimens under their care. We thank the NACOSTI, Kenya for permitting us to carry out our research, and F. K. Manthi and the other staff of the National Museums of Kenya for their assistance in laboratory and fieldwork. This research received support from Agencia Estatal de Investigación (Spanish Ministerio de Economía y Competitividad: PID2020-116908GB-I00, MINECO/FEDER, EU). This study was supported by Basic Science Research Projects from The Sumitomo Foundation (Grant in number, 2300366), and JSPS KAKENHI Grant Number JP 24K021108 and 19KK0188. M.P. has received funding from the postdoctoral fellowships programme Beatriu de Pinós (ref. 2022 BP 00265), funded by the Secretary of Universities and Research (Government of Catalonia) and by the Horizon 2020 programme of research and innovation of the European Union under the Marie Skłodowska-Curie grant agreement No 801370.

1. Introduction

Nacholapithecus kerioi from the Middle Miocene (16−15 Ma) of the Aka Aitheputh Formation in Kenya is represented by abundant postcranial fossils. Their morphology suggests that the body plan of *N. kerioi* was similar to that of primitive apes, which do not specialize in suspensory locomotion, and that this taxon generally engaged in arboreal quadrupedalism (Nakatsukasa et al., 1998; Ishida et al., 2004; Nakatsukasa et al., 2007; Nakatsukasa and Kunimatsu, 2009; Almécija et al., 2021; Pina et al., 2021; Pina and Nakatsukasa, 2024). However, some forelimb features suggest a derived locomotor pattern indicative of incipient forelimb dominance (Nakatsukasa et al., 1998, 2004, 2007, 2012; Ishida et al., 2004; Takano et al., 2018, 2020). For example, KNM-BG 35250 has a bulbous and rounded humeral capitulum, which contributes to the stabilization of the elbow during pronation/supination movements (Ishida et al., 2004; Takano et al., 2018). Overall, *N. kerioi* may mainly relied on cautious arboreal quadrupedalism, occasionally engaging in some other kind(s) of anti-pronograde locomotor modes.

For reconstructing the locomotor repertoire of extinct taxa, the internal morphology of long bones plays a key role because it is influenced by the daily activity patterns throughout an individual's lifetime (Frost, 1980, 1982; Carter, 1984; Pearson and Lieberman, 2004; Ruff et al., 2006; Sugiyama et al., 2010 Warden et al., 2014; Sarringhaus et al., 2016; Canington et al., 2018).

In particular, the femoral neck is a relevant part of the locomotor performance in primates since it bears loadings caused by body weight and contraction of muscles around the hip joint (Lovejoy et al., 1973; 1988; Ruff, 1995; Rafferty, 1998; Harmon, 2007). The femoral neck cortical bone (FNCB) distribution has received great attention in studies of living and extinct apes and humans (Lovejoy et al., 1973; Ohman et al., 1997; Rafferty, 1998; Kuperavage et al., 2010; Demes et al., 2000; Matsumura et al., 2010; Lovejoy et al., 2002; Galik et al., 2004; Pina et al., 2012, 2019; Ruff and Higgins, 2013; Ruff et al., 2016; Cazenave et al., 2019; Friedl et al., 2019; among others). Specifically, the thickness of the superior cortex (SUP) of the femoral neck relative to that of the inferior cortex (INF) has been used to infer loading patterns in primate locomotor behavior. The thicknesses of SUP and INF are similar in extant apes (Galik et al., 2004; Kuperavage et al., 2010; Matsumura et al., 2010). This homogeneous FNCB distribution is explained by multi-directional loadings induced during anti-pronograde locomotor modes, such as clambering or vertical climbing. These multi-directional loadings can be related to the higher degree of hip joint mobility, a common adaptation in ape taxa that navigate arboreal spaces where substrates are distributed three-dimensionally. Accordingly, the morphology of the proximal femur shows great affinity with high ranges of hip joint mobility (Hammond, 2013, 2014; Hammond et al., 2016; Aguilar et al., 2022). Contrastingly, monkeys (except the suspensory atelines) exhibit thinner SUP relative to the INF (heterogeneous distribution), which may be linked to more stereotyped loading patterns

in pronograde quadrupedalism (Ohman et al., 1997; Rafferty, 1998; Demes et al., 2000). Humans also exhibit heterogeneous FNCB distribution (thinner SUP) linked to the human-specific stress pattern in the femoral neck. In this case, the bending force generated by the body weight plus the axial compression caused by the contraction of the abductor muscles during a single leg-support phase produces minimal tension at the SUP and maximum compression at the INF (Lovejoy, 1988; Galik et al., 2004; Kuperavage et al., 2010; Ruff and Higgins, 2013). This fact is of special relevance in human locomotor evolution because the condition of the FNCB distribution gives functional and biomechanical insights into the locomotor behavior of fossil hominins (Ruff and Higgins, 2013; Ruff et al., 2016; Cazenave et al., 2019; Friedl et al., 2019).

While the FNCB distribution has been studied in various living primates and fossil hominins, data on fossil apes is limited to the European dryopiths. Pina et al. (2012, 2019) investigated the FNCB distribution in *Dryopithecus* (11.9 Ma) and *Hispanopithecus* (9.6 Ma) from the Miocene of Spain. They showed that *Dryopithecus* and *Hispanopithecus* exhibit heterogeneous and homogeneous FNCB patterns, respectively (Pina et al., 2012, 2019). The observed FNCB distributions are consistent with the locomotor patterns of these apes inferred from the postcranial external morphology. As to *Dryopithecus*, the heterogeneous FNCB distribution is consistent with the hypothesis that this extinct ape mainly engaged in above-branch quadrupedalism and cautious climbing, and was not adapted to suspensory locomotor behaviors;

while *Hispanopithecus* was more specialized for forelimb-dominated orthograde behaviors, such as below-branch suspension (Moyà-Solà and Köhler, 1996; Moyà-Solà et al., 2009; Alba et al., 2011; Almécija et al., 2021). No study has investigated the FNCB distribution in earlier African fossil apes to date.

The anatomical features of *N. kerioi* cranium provide sufficient support for its phylogenetic position. The loss of the subarcuate fossa in *N. kerioi* (Kunimatsu et al., 2019), as well as its dentognathic features (Nakatsukasa and Kunimatsu, 2009), strongly suggests it is more closely related to the last common ancestor of extant hominids than hylobatids are, although the dispute over its phylogenetic position continues (e.g., Pugh, 2022). Compared to earlier Miocene stem hominoids, such as *Ekembo*, *N. kerioi* shares various derived dental and postcranial features with the extant great apes (Nakatsukasa et al., 1998; Ishida et al., 2004; Nakatsukasa et al., 2007).

Original evidence from the internal morphology of *N. kerioi* could provide further information about the biomechanical hip joint condition in Miocene apes. Here we report the FNCB distribution of *N. kerioi*. Although some derived features can be found in the postcranial remains of *N. kerioi*, they do not necessarily mean they are an adaptation to the extant ape-like suspensory locomotion. In the case of the hind limb, the femur of *N. kerioi* still shows a generally primitive external morphology and, therefore, we hypothesize that the internal architecture of this bone may reflect the presence of a stereotypical loading conditions at the hip joint in this taxon

(Pina et al., 2021), similar to that of pronograde quadrupeds. To test this hypothesis, we compare the distribution of the FNCB in *N. kerioi* with that of pronograde and anti-pronograde extant primates and other extinct hominoids (i.e., European dryopiths).

2. Materials and methods

This study examined X-ray images taken with computed tomography (CT) for four likely male femoral specimens of *Nacholapithecus* (Fig. 1; see also Pina et al., 2019, and Kikuchi et al., 2018 for sex determination). Those images are part of a CT data archive generated over the years by the Nachola Research Team. Because images used in this study were obtained in 2002 and 2014, they were not taken simultaneously and with the purpose of this study. These specimens were CT-scanned using a peripheral quantitative computed tomography scanner (Stratec Medizintechnik GmbH, XCT Research SA) at the National Museums of Kenya (Nairobi), with a pixel size of 50 μm. The femur was positioned in the scanner in a way that the scanned plane was orthogonal to the main mediolateral axis of the neck. Two sections of interest were identified—one running through the most medial part of the greater trochanter, and the other along the lateral edge of the femoral head articular surface on the posterior side. The CT image was taken at the mid-neck level defined as the midpoint between these two planes (Fig. 1; Pina et al., 2012). Nonetheless, it is known that the FNCB distribution changes along the mediolateral axis of the

femoral neck in humans and chimpanzees (Cazenave et al., 2019) and its distribution at the base of the neck better distinguishes bipedalism from extant ape-like locomotor modes (Ruff and Higgins, 2013). Base-of-the-neck CT images were not originally taken. The precise position of the cross-section could not be retrieved digitally from the CT operating system. To overcome this issue, we laser-scanned the original specimens using a NextEngine three-dimensional (3D) scanner (NextEngine Inc., Santa Monica, USA) at the Macro and HD (high point density) settings. Next, we located the best-fit plane for each CT image on the 3D model and fitted results are available in Supplementary Online Material (SOM) Files S1–S4. It is worth noting that all four specimens displayed varying degrees of postmortem damage. One of the specimens only preserves the head and neck portion (KNM-BG 17821), while the neck of another specimen (KNM-BG 35250A) is drastically distorted (see below). Therefore, we examined whether the CT-scanned sections align with the mid-neck point that would be defined in an intact state. We virtually superimposed KNM-BG 42738/42756C, which retains its original form (Kikuchi et al., 2018; Pina et al., 2021), onto those damaged specimens (Fig. 1B and D), using head size as a reference for the 3D renderings superimposition. Then, we compared the position of the CT-scanned section with the mid-neck level defined on the KNM-BG 42738/42756C 3D rendering (Fig. 1; SOM Files S1–S4). While the proximal portion of KNM-BG 42738/42756C is relatively well preserved, the surface cortex layer is partially broken around the mid-neck inferiorly (Fig.

2A; SOM Fig. S1). This cortical defect was manually filled up with plasticine on the original specimen (SOM Fig. S1), and the repaired specimen was scanned with the laser scanner. Then the obtained external surface data was overlaid on the original CT image to draw the external bone boundaries (Fig 2A). In this region, a small section of the internal cortex border is also missing. This small gap was resolved by spline interpolation.

KNM-BG 42738/42756C is a relatively well-preserved left proximal femur (Fig. 1A, SOM Fig. S1). While the femoral head size is well within the range of adult males (Kikuchi et al., 2018), the distal fragment of the KNM-BG 42738/42756C femur shows an incomplete fusion of the distal epiphysis (Pina et al., 2021), suggesting that this femur may belong to a young adult specimen.

KNM-BG 17821 is an isolated right head and neck (Fig. 1B; SOM Fig. S2).

KNM-BG 38391A retains the proximal shaft and allows for investigating the head-neck portion without relying on KNM-BG 42738/42756C (Fig. 1C; SOM File S3). It is associated with a detached tibial proximal epiphysis (KNM-BG 38391C) (unpublished).

KNM-BG 35250A is a right-half proximal femur and belongs to the holotype specimen. When the 3D model of KNM-BG 35250A is superimposed onto that of KNM-BG 42738/42756C (Fig. 1D; SOM File S4), it becomes evident that the position of the greater trochanter differs significantly between the two individuals. This is because KNM-BG 35250A has a shorter

femoral neck. Although previous studies (Nakatsukasa et al., 2012; Pina et al., 2021) warned about the influence of plastic deformation on KNM-BG 35250A, this visual comparison evidences the strong distortion in this fossil femur. The femoral head of KNM-BG 35250A is displaced distally towards the neck, and its articular surface bulges noticeably over the neck (SOM Fig. S4). Due to this deformation, the proximal neck is truncated. Therefore, the CT section was taken at a rather lateral level from the base of the neck in its inferred undeformed condition. This explains why the tip of the greater trochanter is visible on the top of the neck and why the superoposterior part of the cortex is extremely thin unlike other specimens (Fig. 2D). Thus, this specimen was excluded from the analysis.

In each CT image, the most superior and inferior points of the external cortical surface were determined, and SUP and INF thicknesses were measured on the line connecting these points following previous studies (Pina et al., 2012; Ruff and Higgins, 2013) by using Photoshop v. 21.1 (Adobe, San José; Fig. 2). To assess inter-observer differences, these measurements were taken by two well-trained additional observers (SOM Table S1). Considering the standard deviation of the observer's measurements, inter-observer differences do not have a significant effect on our results. In addition to SUP and INF thicknesses, anterior and posterior cortical thicknesses were measured in KNM-BG 42738/42756C and KNM-BG 17821 following the below protocol. An anteroposterior axis was defined as an orthogonal line to a superoinferior axis passing through the

mid-point between the superior and inferior points of the external cortical surface. These measurements were not analyzed in this study because of the lack of comparative data but are here documented for future studies.

The dataset of comparative taxa represents a subset of the data published in Pina et al. (2019). This dataset includes *Pan troglodytes*, *Gorilla gorilla*, *Pongo pygmaeus*, *Hylobates lar*, *Symphalangus syndactylus*, cercopithecids, atelids, strepsirrhines, *Dryopithecus fontani* (IPS41724) and *Hispanopithecus laietanus* (IPS18800.29). This study uses the same locomotor grouping as in Pina et al. (2019), that is quadrupeds, slow climbers, suspensory taxa, and knuckle-walkers/vertical climbers. *Nacholapithecus* was compared against these categories. Analyses were performed using Excel v. 2019 (Microsoft, Redmond.).

3. Results

The cortex in KNM-BG 42738/42756C is well discriminated from the trabecular bone anteriorly, posteriorly, and posteroinferiorly (Fig. 2A). Horizontal band-like dark zones are present in the anterior cortex. These lower-density areas seem CT artifacts. SUP exhibits many dark grey spots/dots and is distinct from the other cortical regions. A few of those spots are relatively large and elongated. Most of the spots are apparently distinguished from inter-trabecular space in the medullary cavity in terms of size. The largest ones located superoposteriorly may be

oblique sections of vascular canals (Fig. 2A inset, arrow). More superficial dark areas just beneath the external surface are likely damaged. Neck metrics are shown in Table 1.

The cross-sectional profile of KNM-BG 17821 is ellipsoidal like that of KNM-BG 42738/42756C (Table 1: Neck diameter ratio). In the CT image, the cortex can be clearly discriminated from the medullary cavity (Fig. 2B). However, the SUP is cracked, and some of those cracks appear to reach the medullary cavity. There is a marked local thickening of the whitish area superiorly (Fig. 2B inset, arrow). This may indicate a cortical bone piece that was fractured and displaced. The external surface corresponding to this part is rugose due to postmortem damage (SOM Fig. S2B inset). Because the internal cortical border is ambiguous in this part, the boundary of the SUP was marked conservatively (Fig. 2B). The cortical bone is thicker all around compared to KNM-BG 42738/42756C resulting in a higher relative cortical area (Table 1: 0.40 vs. 0.34), and the trabecular mesh appears denser.

The CT section of the neck in KNM-BG 38391A differs significantly from that of KNM-BG 42738/42756C and KNM-BG 17821. The external profile is narrower anteroposteriorly (Table 1: Neck diameter ratio). In addition, the cortical bone is quite thinner superiorly and superoposteriorly (Fig. 2C; Table 1). The external profile of these regions is wavy. Close observation of the original specimen identifies the flaking of cortical bone on the external surface of the femoral neck (SOM Fig. S3). In the superior and superoposterior cortex, cross sections of

canals are observed. Within the anterior part of the cortex, there is a slightly darker area, possibly caused by some microfractures. Other than this, there are a few gray crack lines in the anterior cortex. In addition, trabeculae are probably fractured under the anterior cortex (Fig. 2C inset). For these reasons, the specimen was not suitable for measuring and was excluded from the analysis.

The SUP/INF index of the *Nacholapithecus* femora is 0.85 for KNM-BG 42738/42756C and 0.82 for KNM-BG 17821 (Table 1). These values are in the range of the averages of suspensory taxa and African apes (Fig. 3). As explained above, noticeable lower values of KNM-BG 38391A and KNM-BG 35250A (Table 1) are not considered for discussion below.

4. Discussion and conclusions

In this study, we quantified the FNCB distribution at the mid-neck of four *Nacholapithecus* femora (attributed to males; Kikuchi et al., 2018). Despite the studied specimens showing postmortem damage on the FNCB and only two CT images being usable, the present study provides new evidence that adds to the knowledge of the locomotor behavior of *Nacholapithecus* and the functional significance of the SUP/INF index, being the first time data on the internal structure of the femoral neck is reported for an African extinct ape. The homogeneous distribution of the FNCB in *Nacholapithecus* supports the hypothesis that the loading conditions in the femoral neck of this taxon is multi-directional. These results contrast

with previous observations on the external morphology of the *Nacholapithecus* femur, which is relatively primitive mainly at the proximal end (Pina et al., 2021). For instance, the relative head size based on the neck is moderate, the neck is relatively long, and the neck shaft angle is moderate compared with extant suspensory taxa (Pina et al., 2021: Fig. 6). All these traits suggest that the femur lacks features related to enhanced hip joint mobility and is less adapted to anti-pronograde locomotor behaviors, unlike orangutans and gibbons. However, other postcranial remains (e.g., forelimb bones) suggest that the locomotor repertoire of *Nacholapithecus* included a combination of generalized arboreal quadrupedalism and anti-pronograde behaviors, like clambering (Nakatsukasa and Kunimatsu, 2009; Nakatsukasa et al., 2012; Takano et al., 2018, 2020; Pina et al., 2021; Arias-Martorell et al., 2023; Pina and Nakatsukasa, 2024).

Postcranial skeletal morphology may permit some level of behavioral flexibility because most living primate species utilize more than one locomotor mode so their skeletal morphology must be a compromise to deal with the different biomechanical requirements of those behaviors (see Rose, 1991). While the morphology of the femoral neck, especially the neck-shaft angle, is a good indicator of hip joint mobility (abduction and lateral rotation, for instance) in living primates (Aguilar et al., 2022), the relationship is not straightforward in fossil apes. Using fossil remains to infer locomotor modes is complex because of the mosaic nature of some taxa. For example, Early Miocene *Ekembo* exhibits a high femoral neck-shaft angle, but its pelvis does not

show the extant ape-like feature set related to anti-pronograde postures during locomotion (Ward et al., 1993).

Results of this study suggest that *Nacholapithecus* used its thigh in non-stereotyped ways, probably in relation to a higher degree of anti-pronograde behaviors compared to extant pronograde primates. Considering the derived features of forelimb and foot bones (Nakatsukasa et al., 2012; Takano et al., 2018, 2020; Arias-Martorell et al., 2023; Pina and Nakatsukasa, 2024), *Nacholapithecus* might have engaged in anti-pronograde locomotion (e.g. clambering, transferring, and bridging) and orthograde-like postures regularly rather than occasionally.

Dryopithecus (IPS41724) exhibits heterogeneous FNCB distribution (Pina et al., 2019). This suggests that the locomotor behavior in *Dryopithecus* was less derived compared to *Nacholapithecus* or, at least, loadings were distributed through the femoral neck in a more stereotyped pattern. Contrarily, the value of the SUP/INF index in *Nacholapithecus* is lower than that of *Hispanopithecus* (IPS18800.29). These two taxa also differ regarding other femoral neck cross-sectional features. For instance, the femoral neck cross-section shape is elongated superoinferiorly in *Nacholapithecus* (Fig. 2), whereas it is more circular in *Hispanopithecus* (Pina et al., 2019: Fig. 4b) suggesting, together with other external morphology traits of the proximal end of the femur, different loading environments for these two taxa. In addition, the cortical bone is clearly thicker in *Hispanopithecus*. The femoral neck of *Nacholapithecus* could suggest a more

stereotyped loading pattern compared to the latter taxon.

However, the idea of a dichotomy of homogeneous/heterogeneous FNCB distribution might be too simplistic to reconstruct locomotor behavior in extinct primates (Rafferty, 1998; Pina et al., 2019). While the relative cortical area (cortical area/total area) is ≤ 0.40 in *Nacholapithecus* (Table 1), it is 0.55 in *Hispanopithecus* (144 mm^2/264 mm^2: calculated from Pina et al., 2019: Fig. 4b). This difference may suggest that the stress levels at the neck were different between the two species. Whether it is related to the differences in body mass (22 kg in *N. kerioi*; Kikuchi et al., 2018; 39 kg in *Hispanopithecus*; Moyà-Solà et al., 2009), body mass fraction supported by the hind limb, or kinematics of the hip joint (or any combination) is to be explored.

In summary, this study provides support to the hypothesis that *Nacholapithecus* engaged in a higher degree of anti-pronograde behaviors compared to extant pronograde primates through an examination of the two-dimensional data of the FNCB distribution. It highlights the significance of analyzing bone internal structure to make functional inferences in fossil primates. As all the studied specimens showed postmortem damage on the cortical bone, it would be beneficial to conduct a future study with a focus on the 3D (along the femoral neck) distribution of FNCB, particularly comparing antero-posterior thicknesses. This would also improve the potential issue of locating the CT sections. Ruff and Higgins (2013) found that the base-of-the-neck section offers a clearer functional signal than the mid-neck section in extant and extinct

hominins. This may be related to laterally increasing bending stress, assuming the beam cantilever model of the femoral neck. Additionally, lateral to medial change of cortex distribution (decreasing asymmetry of SUP/INF and the thickness of anterior and posterior cortices) was suggested as a character that reflects gait kinematics in extinct hominins (Cazenave et al., 2019). If volumetric internal structural data of the femoral neck is acquired in the future, 3D cortical analysis (e.g., following Cazenave et al., 2019) may allow us to more accurately reconstruct the hip joint biomechanics of *Nacholapithecus*.

References

Aguilar, L.K., Collins, C.E., Ward, C.V., Hammond, A.S., 2022. Pathways to primate hip function. Royal Society Open Science 9, 211762.

Alba, D.M., Moyà-Solà, S., Almécija, S., 2011. A partial hominoid humerus from the Middle Miocene of Castell de Barbera (Vallès-Penedès Basin, Catalonia, Spain). American Journal of Physical Anthropology 144, 365-381.

Almécija, S., Hammond, A.S., Thompson, N.E., Pugh, K.D., Moyà-Solà, S., Alba, D.M., 2021. Fossil apes and human evolution. Science 372.

Arias-Martorell, J., Urciuoli, A., Almécija, S., Alba, D. M., Nakatsukasa, M., 2023. The radial head of the Middle Miocene ape *Nacholapithecus kerioi*: Morphometric affinities, locomotor

inferences, and implications for the evolution of the hominoid humeroradial joint. Journal of Human Evolution, 178, 103345.

Carter, D.R., 1984. Mechanical loading histories and cortical bone remodeling. Calcified Tissue International 36 (Suppl. 1), S19-S24.

Canington, S.L., Sylvester, A.D., Burgess, M.L., Junno, J.A., Ruff, C.B., 2018. Long bone diaphyseal shape follows different ontogenetic trajectories in captive and wild gorillas. American Journal of Biological Anthropology 167, 366-376.

Cazenave, M., Braga, J., Oettlé, A., Pickering, T.R., Heaton, J.L., Nakatsukasa, M., Thackeray, J.F., de Beer, F., Hoffman, J., Dumoncel, J., Macchiarelli, R., 2019. Cortical bone distribution in the femoral neck of *Paranthropus robustus*. Journal of Human Evolution 135, 102666.

Demes, B., Jungers, W.L., Walker, C., 2000. Cortical bone distribution in the femoral neck of strepsirhine primates. Journal of Human Evolution 39, 367-379.

Fajardo, R.J., Müller, R., 2001. Three-dimensional analysis of nonhuman primate trabecular architecture using micro-computed tomography. American Journal of Physical Anthropology 115, 327-336.

Fajardo, R.J., Müller, R., Ketcham, R.A., Colbert, M., 2007. Nonhuman anthropoid primate femoral neck trabecular architecture and its relationship to locomotor mode. The Anatomical Record 290, 422-436.

Friedl, L., Claxton, A.G., Walker, C.S., Churchill, S.E., Holliday, T.W., Hawks, J., Berger, L.R., DeSilva, J.M., Marchi, D., 2019. Femoral neck and shaft structure in *Homo naledi* from the Dinaledi Chamber (Rising Star System, South Africa). Journal of Human Evolution 133, 61-77.

Frost, H.M., 1980. The "new bone": Some anthropological potentials. American Journal of Physical Anthropology 28, 211-226.

Frost, H.M., 1982. Review article mechanical determinants of bone modeling. Metabolic Bone Disease and Related Research 4, 217–229.

Galik, K., Senut, B., Pickford, M., Gommery, D., Treil, J., Kuperavage, A.J., Eckhardt, R.B., 2004. External and internal morphology of the BAR 1002'00 *Orrorin tugenensis* femur. Science 305, 1450-1453.

Hammond, A.S., 2013. 3D analysis of hip joint mobility and the evolution of locomotor abilities in Miocene hominoids. University of Missouri-Columbia.

Hammond, A.S., 2014. In vivo baseline measurements of hip joint range of motion in suspensory and nonsuspensory anthropoids. American Journal of Physical Anthropology 153, 417-434.

Hammond, A.S., Plavcan, J.M., Ward, C.V., 2016. A validated method for modeling anthropoid hip abduction in *silico*. American Journal of Physical Anthropology 160, 529-548.

Harmon, E.H., 2007. The shape of the hominoid proximal femur: a geometric morphometric

analysis. Journal of Anatomy 210, 170-185.

Ishida, H., Kunimatsu, Y., Takano, T., Nakano, Y., Nakatsukasa, M., 2004. *Nacholapithecus* skeleton from the Middle Miocene of Kenya. Journal of Human Evolution 46, 69-103.

Kikuchi, Y., Nakatsukasa, M., Tsujikawa, H., Nakano, Y., Kunimatsu, Y., Ogihara, N., Shimizu, D., Takano, T., Nakaya, H., Sawada, Y., Ishida, H., 2018. Sexual dimorphism of body size in an African fossil ape, *Nacholapithecus kerioi*. Journal of Human Evolution 123, 129-140.

Kunimatsu, Y., Nakatsukasa, M., Shimizu, D., Nakano, Y., Ishida, H., 2019. Loss of the subarcuate fossa and the phylogeny of *Nacholapithecus*. Journal of Human Evolution 131, 22-27.

Kuperavage, A.J., Sommer, H.J., Eckhardt, R.B., 2010. Moment coefficients of skewness in the femoral neck cortical bone distribution of BAR 1002'00. HOMO: Journal of Comparison Human Biology 61, 244-252.

Lovejoy, C.O., 1988. Evolution of human walking. Scientific American 259, 118-125.

Lovejoy, C.O., Heiple, K.G., Burstein, A.H., 1973. The gait of *Australopithecus*. American Journal of Physical Anthropology 38, 757-779.

Lovejoy, C.O., Meindl, R.S., Ohman, J.C., Heiple, K.G., White, T.D., 2002. The Maka femur and its bearing on the antiquity of human walking: applying contemporary concepts of morphogenesis to the human fossil record. American Journal of Physical Anthropology 119, 97-133.

MacLatchy, L., Müller, R., 2002. A comparison of the femoral head and neck trabecular architecture of *Galago* and *Perodicticus* using micro-computed tomography (microCT). Journal of Human Evolution 43, 89-105.

Matsumura, A., Gunji, H., Takahashi, Y., Nishida, T., Okada, M., 2010. Cross-Sectional Morphology of the Femoral Neck of Wild Chimpanzees. International Journal of Primatology 31, 219-238.

Moyà-Solà, S., Köhler, M., 1996. A *Dryopithecus* skeleton and the origin of great-ape locomotion. Nature 379, 156–159.

Moyà-Solà, S., Köhler, M., Alba, D.M., Casanovas-Vilar, I., Galindo, J., Robles, J.M., Cabrera, L., Garcés, M., Almécija, S., Beamud, E., 2009. First partial face and upper dentition of the Middle Miocene hominoid *Dryopithecus fontani* from Abocador de Can Mata (Vallès-Penedès Basin, Catalonia, NE Spain): Taxonomic and phylogenetic implications. American Journal of Physical Anthropology 139, 126-145.

Nakatsukasa, M., Kunimatsu, Y., 2009. *Nacholapithecus* and its importance for understanding hominoid evolution. Evolutionary Anthropology 18, 103-119.

Nakatsukasa, M., Kunimatsu, Y., Nakano, Y., Ishida, H., 2007. Vertebral morphology of *Nacholapithecus kerioi* based on KNM-BG 35250. Journal of Human Evolution 52, 347-369.

Nakatsukasa, M., Kunimatsu, Y., Shimizu, D., Nakano, Y., Kikuchi, Y., Ishida, H., 2012. Hind

limb of the *Nacholapithecus kerioi* holotype and implications for its positional behavior. Anthropological Science 120, 235-250.

Nakatsukasa, M., Ward, C.V., Walker, A., Teaford, M.F., Kunimatsu, Y., Ogihara, N., 2004. Tail loss in *Proconsul heseloni*. Journal of Human Evolution 46, 777-784.

Nakatsukasa, M., Yamanaka, A., Kunimatsu, Y., Shimizu, D., Ishida, H., 1998. A newly discovered *Kenyapithecus* skeleton and its implications for the evolution of positional behavior in Miocene East African hominoids. Journal of Human Evolution 34, 657-664.

Ohman, J.C., Krochta, T.J., Lovejoy, C.O., Mensforth, R.P., Latimer, B., 1997. Cortical bone distribution in the femoral neck of hominoids: Implications for the locomotion of *Australopithecus afarensis*. American Journal of Physical Anthropology 104, 117-131.

Pearson, O.M., Lieberman, D.E., 2004. The aging of Wolff's "law": ontogeny and responses to mechanical loading in cortical bone. American Journal of Physical Anthropology Suppl 39, 63-99.

Pina, M., Alba, D.M., Almécija, S., Fortuny, J., Moyà-Solà, S., 2012. Brief communication: Paleobiological inferences on the locomotor repertoire of extinct hominoids based on femoral neck cortical thickness: The fossil great ape *Hispanopithecus laietanus* as a test-case study. American Journal of Physical Anthropology 149, 142-148.

Pina, M., Alba, D.M., Moyà-Solà, S., Almécija, S., 2019. Femoral neck cortical bone distribution

of dryopithecin apes and the evolution of hominid locomotion. Journal of Human Evolution 136, 102651.

Pina, M., Kikuchi, Y., Nakatsukasa, M., Nakano, Y., Kunimatsu, Y., Ogihara, N., Shimizu, D., Takano, T., Tsujikawa, H., Ishida, H., 2021. New femoral remains of *Nacholapithecus kerioi:* Implications for intraspecific variation and Miocene hominoid evolution. Journal of Human Evolution 155, 102982.

Pina, M., Nakatsukasa, M., 2024. New quantitative analyses of the *Nacholapithecus kerioi* proximal ulna confirm morphological affinities with Equatorius and large papionins. American Journal of Biological Anthropology 185, e25000.

Rafferty, K.L., 1998. Structural design of the femoral neck in primates. Journal of Human Evolution 34, 361-383.

Pugh, K.D., 2022. Phylogenetic analysis of Middle-Late Miocene apes. Journal of Human Evolution 165, 103140.

Rose, M.D., 1991. The process of bipedalization in hominids. In: Coppens, Y., Senut, B. (Eds), Origine(s) de la Bipédie chez les Hominidés. CNRS, Paris, pp. 37–48.

Ruff, C.B., 1995. Biomechanics of the hip and birth in early *Homo*. American Journal of Physical Anthropology 98, 527-574.

Ruff, C.B., Burgess, M.L., Ketcham, R.A., Kappelman, J., 2016. Limb Bone Structural

Proportions and Locomotor Behavior in A.L. 288-1 ("Lucy"). PLOS ONE 11, e0166095.

Ruff, C.B., Higgins, R., 2013. Femoral neck structure and function in early hominins. American Journal of Physical Anthropology 150, 512-525.

Ruff, C.B., Holt, B., Trinkaus, E., 2006. Who's afraid of the big bad wolff? "Wolff's law" and bone functional adaptation. American Journal of Physical Anthropology 129, 484-498.

Stini, W. A., 1990. “Osteoporosis”: Etiologies, prevention, and treatment. American Journal of Physical Anthropology. 33, 151-194.

Sarringhaus, L.A., MacLatchy, L.M., Mitani, J.C., 2016. Long bone cross-sectional properties reflect changes in locomotor behavior in developing chimpanzees. American Journal of Physical Anthropology 160, 16-29.

Sugiyama, T., Price, J.S., Lanyon, L.E., 2010. Functional adaptation to mechanical loading in both cortical and cancellous bone is controlled locally and is confined to the loaded bones. Bone 46, 314-321.

Takano, T., Nakatsukasa, M., Kunimatsu, Y., Nakano, Y., Ogihara, N., Ishida, H., 2018. Forelimb long bones of *Nacholapithecus* (KNM-BG 35250) from the middle Miocene in Nachola, northern Kenya. Anthropological Science 126, 135-149.

Takano, T., Nakatsukasa, M., Pina, M., Kunimatsu, Y., Nakano, Y., Morimoto, N., Ogihara, N., Ishida, H., 2020. New forelimb long bone specimens of *Nacholapithecus kerioi* from the

Middle Miocene of northern Kenya. Anthropological Science 128, 27-40.

Ward, C.V., Walker, A., Teaford, M.F., Odhiambo, I., 1993. Partial skeleton of *Proconsul nyanzae* from Mfangano Island, Kenya. American Journal of Physical Anthropology 90, 77-111.

Warden, S.J., Mantila Roosa, S.M., Kersh, M.E., Hurd, A.L., Fleisig, G.S., Pandy, M.G., Fuchs, R.K., 2014. Physical activity when young provides lifelong benefits to cortical bone size and strength in men. Proc Natl Acad Sci U S A 111, 5337-5342.

Figure captions

Figure 1. Surface renderings of *Nacholapithecus* femora in the posterior view. A) KNM-BG 42738/42756C; B) KNM-BG 17821; C) KNM-BG 38391A; D) KNM-BG 35250A. KNM-BG 17821 and KNM-BG 35250A (mirrored) are superimposed over the reference femur KNM-BG 42738/42756C, which is represented by a transparent grey color. In each specimen, the main axis of the neck, the most medial edge of the greater trochanter and the lateral edge of the femoral head are shown by black lines. The closed circle on the main axis of the neck indicates the mid-neck point. For KNM-BG 17821 and KNM-BG 35250A, these lines are determined based on the superimposed KNM-BG 42738/42756C. The orange line marks the position where the original CT image was taken. Scale bar: 10 mm.

Figure 2. Computed tomography images of the femoral neck in four *Nacholapithecus* specimens. A) KNM-BG 42738/42756C; B) KNM-BG 17821; C) KNM-BG 38391A; D) KNM-BG 35250A. In each image, left and right correspond to posterior and anterior, respectively (shown as arrow; S: superior, P: posterior). Top row: original images. Bottom row: those with auxiliary lines to define cortical thickness (white) and the trace of the cortical boundary (black). The red line connects the most superior and inferior points on the external surface. The superior and inferior cortical thicknesses were measured along this line. Inset in A: Close-up view of the porous cortical area. Large pores may be oblique sections of a vascular canal (arrowhead). Inset in B: Close-up view of the cracked superior cortex. Inset in C: fractured trabecular bones. In the KNM-BG 35250A (Fig. 2D), the great trochanter is seen over the neck cortex (white arrowhead). Scale bar: 10 mm.

Figure 3. Box-and-whisker plots of superior to inferior cortical thickness ratio (SUP/INF) in extant primates compared with fossil data. For extant species, species averages were grouped

according to locomotor groups. Closed circle: *Dryopithecus* (IPS41724); black open circle: *Hispanopithecus* (IPS18800.29). *Nacholapithecus* specimens are indicated by squares (estimated value for KNM-BG 42738/42756C). Data other than that of *Nacholapithecus* were adopted and modified from Pina et al. (2019). Red line is the median, boxes show the interquartile range between the 25th and the 75th percentiles, whiskers represent 1.5 times the interquartile ranges, and red open circles are outlier. Abbreviations: Q = quadrupeds; SC = slow climbers; SUS = suspensory taxa; KW = knuckle-walkers.

Figure1

Click here to access/download;Figure;FIg1_v5.tif

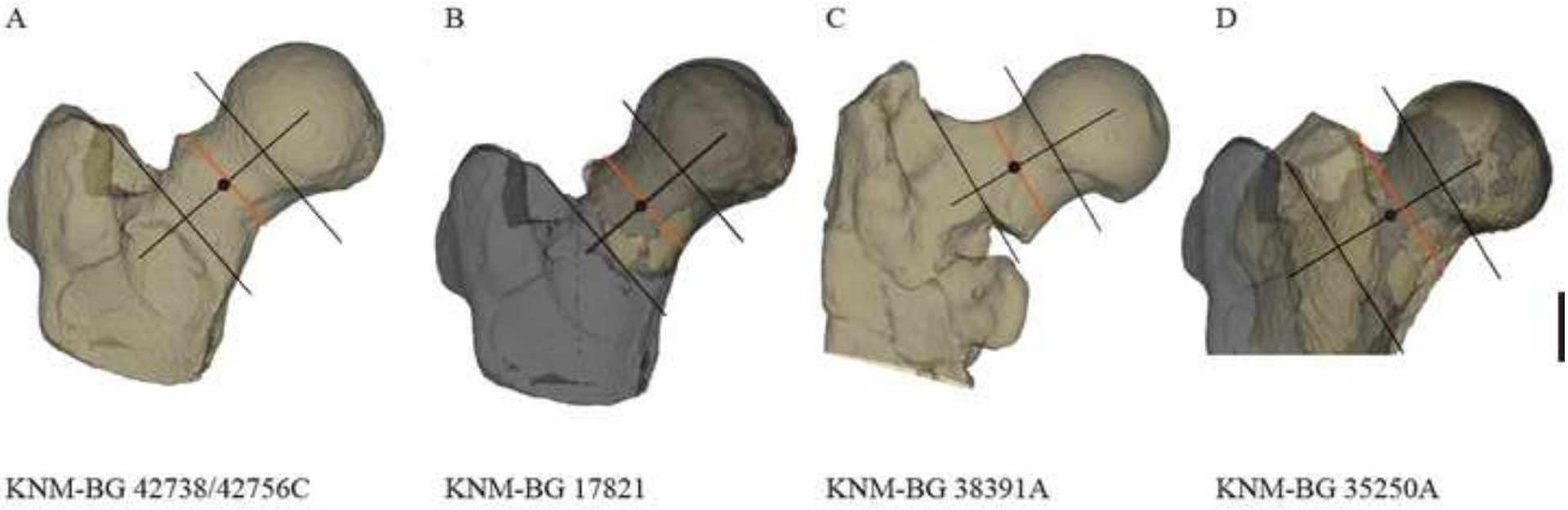

Figure2

Click here to access/download;Figure;fig2_R1.tif

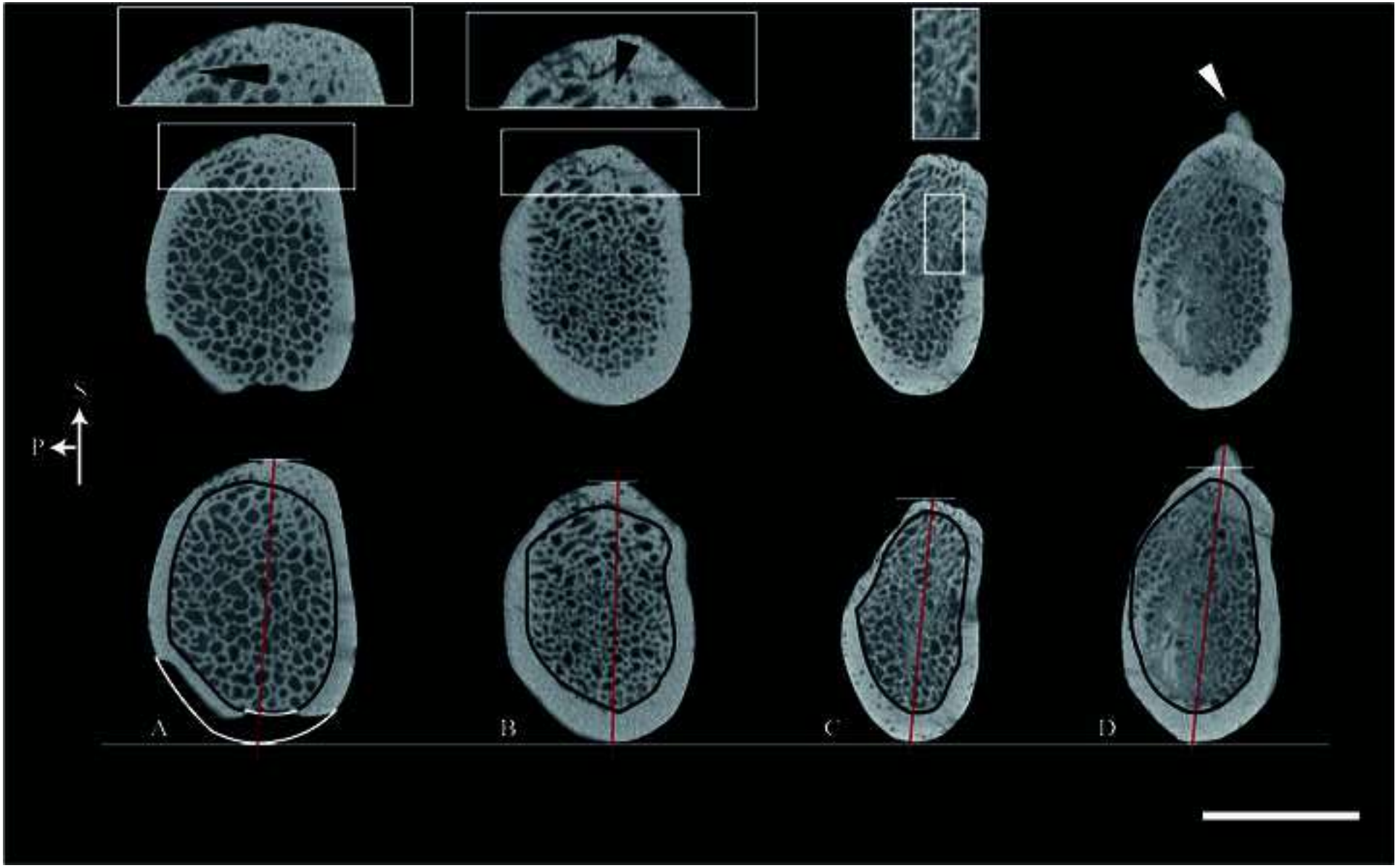

Figure3

Click here to access/download;Figure;fig3_R1.tif

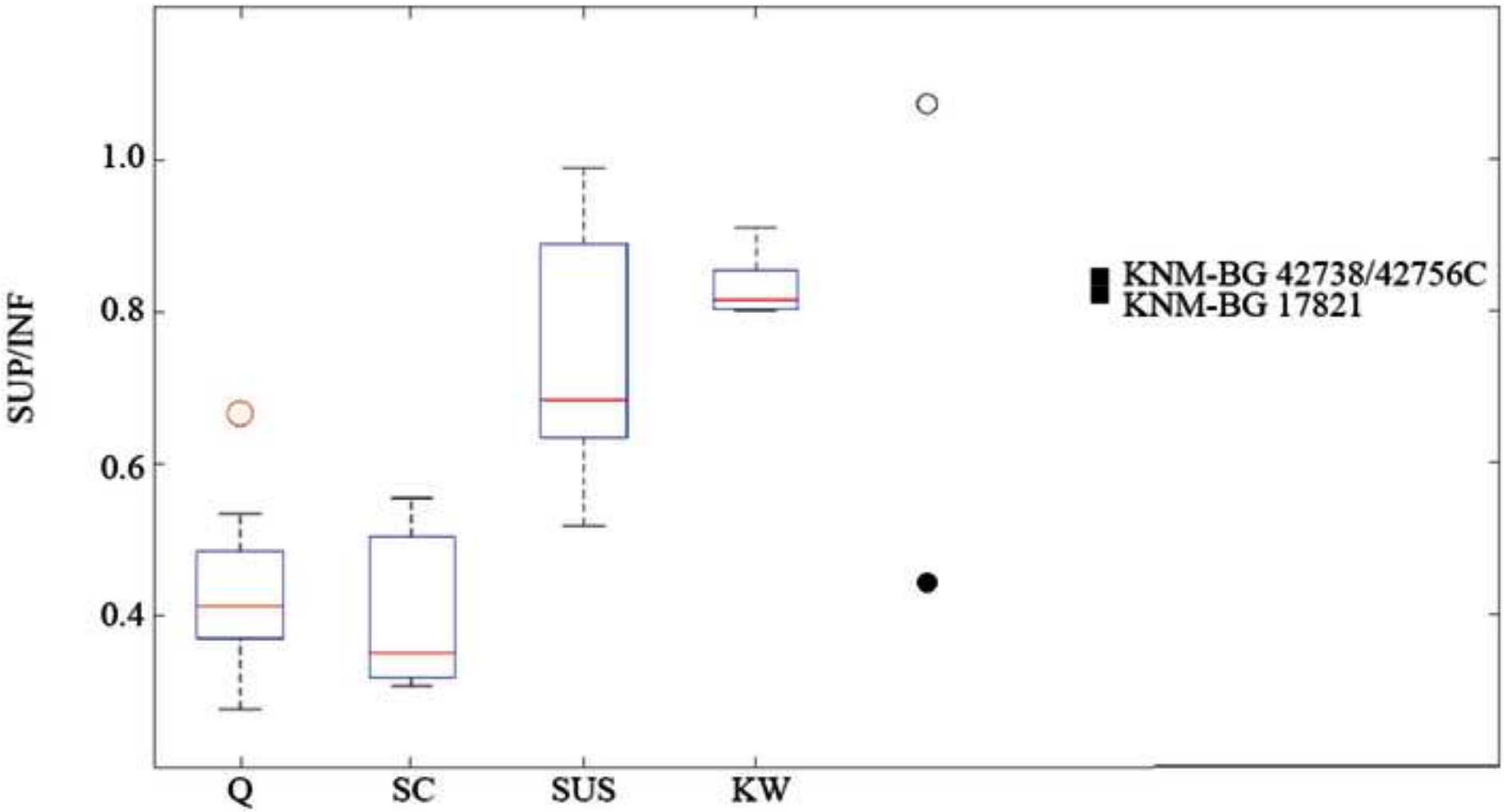

Table 1

Quantitative data of *Nacholapithecus* femoral neck. INF, Inferior cortical thickness; SUP, Superior cortical thickness; TA, Total area.

Specimen	Superoinferior diameter (mm)	Anteroposterior diameter (mm)	Neck diameter ratio	SUP (mm)	INF (mm)	SUP/INF	Anterior cortical thickness (mm)	Posterior cortical thickness (mm)	TA (mm^2)	Cortical area/TA
KNM-BG 42738/42756C	18.1	13.5	0.75	1.73	2.05[a]	0.85	1.30	1.27	193[a]	0.34
KNM-BG 17821	16.7	12.1	0.72	1.80	2.18	0.82	1.44	1.51	164	0.40
KNM-BG 38391A	15.6	8.9	0.57	0.95[b]	1.98	0.48[b]	—	—	—	—
KNM-BG 35250A	17.6	10.1	0.57	0.96[b]	2.05	0.47[b]	—	—	—	—

[a] Estimated values.

[b] Values unsuitable for study.

Supplementary Online Material (SOM):

Femoral neck cortical bone distribution in *Nacholapithecus* from the Middle Miocene of Kenya

SOM Figure S1. Photographs of KNM-BG 42738/42756C. In the close-up view, a wavy external surface with mediolaterally extending shallow furrows is observed. In each pair of the middle and bottom rows, the right image shows the condition after repair of the mid-neck junction (arrow). Whereas the proximal shaft is anteroposteriorly compressed during the fossilization process, the head and the proximal part of the neck do not seriously suffer from plastic deformation.

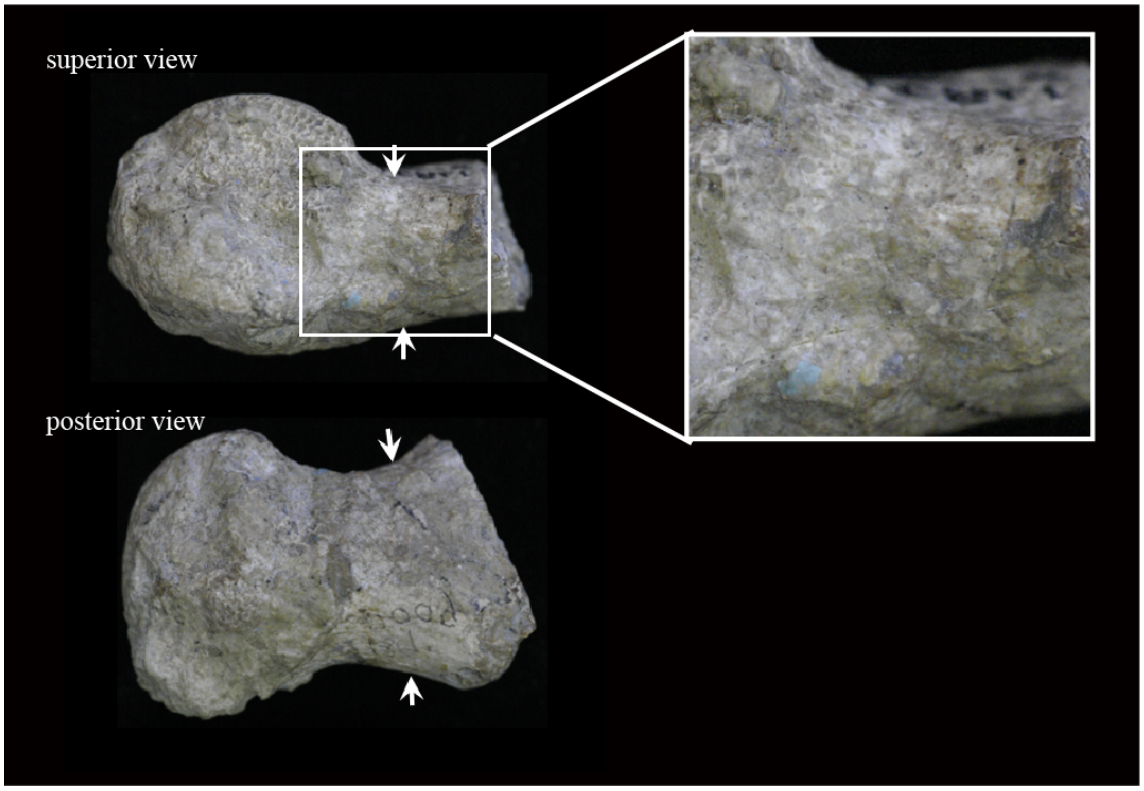

SOM Figure S2. KNM-BG 17821 (mirror image) in superior and posterior views. Arrows indicate CT scanned position. In the close-up image, the wavy surface texture suggests that the surface cortex is damaged.

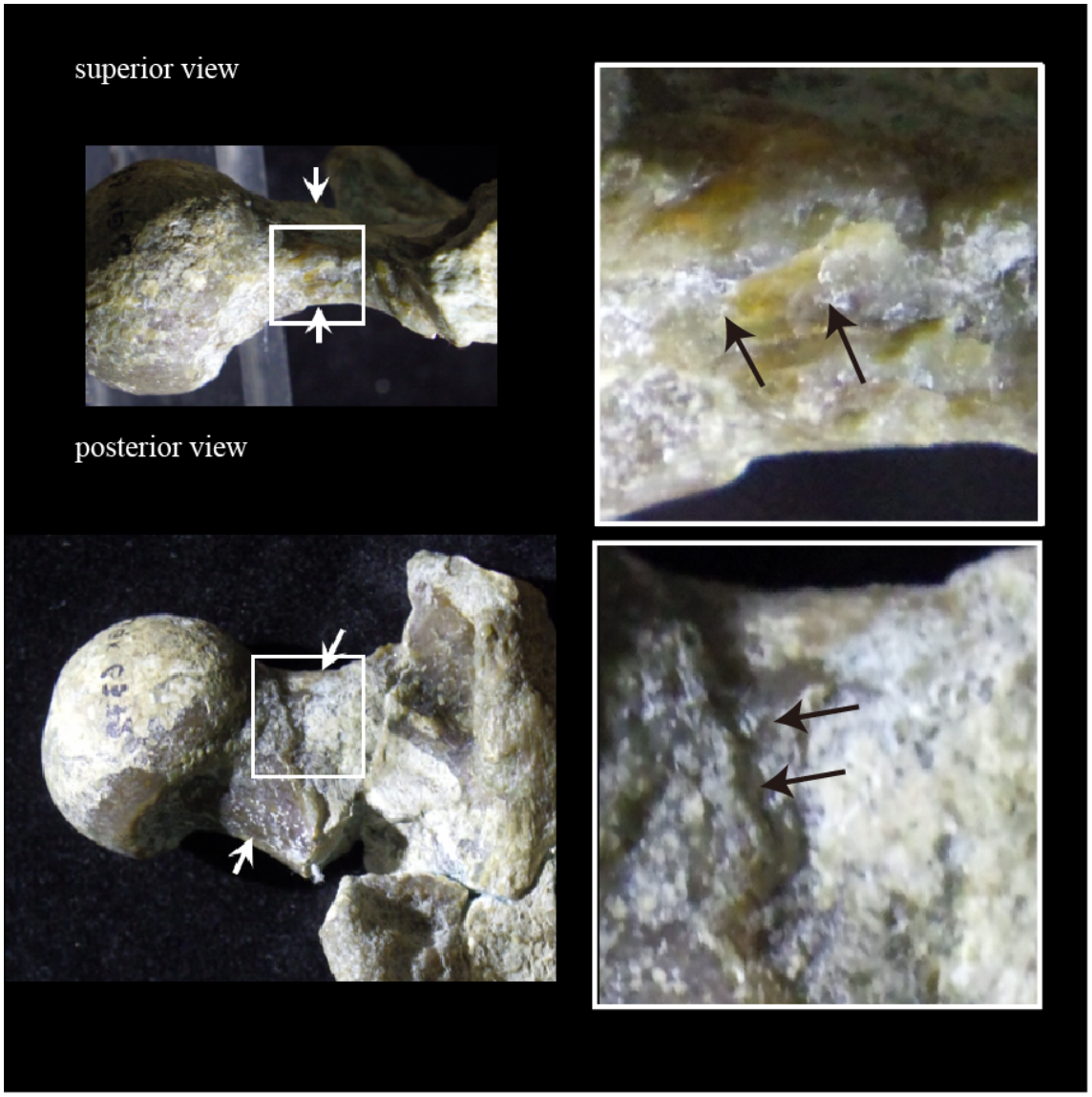

SOM Figure S3. Superior and posterior views of KNM-BG 38391A (mirror image). White arrows show the CT-scanned position. In the close-up windows, surface damages are highlighted by black arrows.

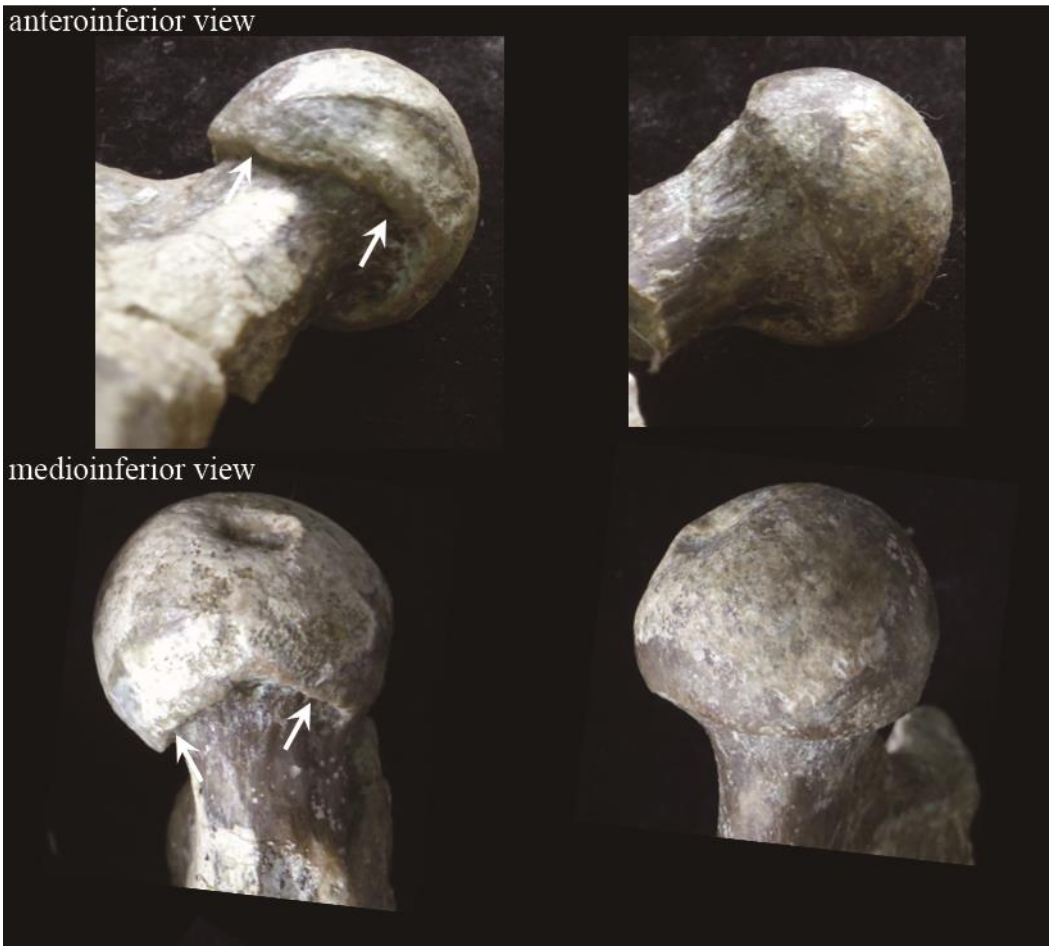

SOM Figure S4. Morphological comparisons of the femoral head between KNM-BG 35250A (left) and KNM-BG 42738/42756C (right). Arrows indicate unusual bulging of the articular surface over the neck in KNM-BG 35250A.

SOM File S1. Three-dimensional rendering of KNM-BG 42738/42756C (red-colored) showing the CT-scanned position (green-colored). To see transparent rendering, use the 'x-ray shader' option in MeshLab (Render -> Shaders -> ray.gdp). Provided as a separate .PLY file.

SOM File S2. Three-dimensional rendering of KNM-BG17821 (red-colored) superimposed on KNM-BG 42738/42756C (green-colored). The CT-scanned position in KNM-BG17821 is also shown. Provided as a separate .PLY file.

SOM File S3. Three-dimensional rendering of KNM-BG 38391A (red-colored) showing the CT-scanned position (green-colored). Provided as a separate .PLY file.

SOM File S4. Three-dimensional rendering of KNM-BG35250A (red-colored) superimposed on KNM-BG 42738/42756C (green-colored) after size adjustment. The CT-scanned position in KNM-BG 35250A is also shown. Provided as a separate .PLY file.

SOM Table S1. Average and standard division of the three measurements on the two CT slices.

	First Author	Observer 1	Observer 2	Mean	SD
SUP_KNM-BG 42738/42756C	1.73	1.49	1.42	1.55	0.16
INF_KNM-BG 42738/42756C	2.05	1.85	1.63	1.84	0.21
SUP/INF_ KNM-BG 42738/42756C	0.85	0.81	0.87	0.84	0.03
SUP_KNM-BG 17821	1.80	1.96	1.30	1.69	0.34
INF_KNM-BG 17821	2.18	2.14	2.01	2.11	0.09
SUP/INF_ KNM-BG 17821	0.82	0.92	0.64	0.79	0.14

SUP: superior cortical thickness, INF: inferior cortical thickness.